ACS OMEGA

http://pubs.acs.org/journal/acsodf

Article

Silver-Doped Cadmium Selenide/Graphene Oxide-Filled Cellulose Acetate Nanocomposites for Photocatalytic Degradation of Malachite Green toward Wastewater Treatment

Mohamed K. Ahmed,* Ahmed Esmail Shalan,* Mohamed Afifi,* Mohamed M. El-Desoky,* and Senentxu Lanceros-Méndez*

Cite This: *ACS Omega* 2021, 6, 23129−23138

Read Online

ACCESS | Metrics & More | Article Recommendations | Supporting Information

ABSTRACT: Silver-doped cadmium selenide/graphene oxide (GO) (Ag-CdSe/GO) nanocomposites have been synthesized, loaded in cellulose acetate (CA) to form Ag-CdSe/GO@CA heterostructure nanofibers, and characterized in terms of structural, morphological, photocatalytic properties, among others. The photocatalytic degradation of malachite green (MG) was estimated using cadmium selenide-filled CA (CdSe@CA), silver-doped cadmium selenide-filled CA (Ag-CdSe@CA), cadmium selenide/GO-filled CA (CdSe/GO@CA), and silver-doped cadmium selenide/GO-filled CA (Ag-CdSe/GO@CA) nanocomposite materials. The Ag-CdSe/GO@CA nanocomposites exhibit and retain an enhanced photocatalytic activity for the degradation of MG dye. This amended performance is associated with the multifunctional supporting impacts of GO, Ag, and CA on the composite structure and properties. The superior photocatalytic activity is related to the fact that both Ag and GO can act as electron acceptors that boost the separation efficiency of photogenerated carriers and the loading of the combined nanocomposite (Ag-CdSe@GO) on CA nanofibers, which can augment the adsorption of electrons and holes and facilitate the movement of carriers. The stability of Ag-CdSe/GO@CA nanocomposite photocatalysts demonstrates suitable results even after five recycles. This study establishes an advanced semiconductor-based hybrid nanocomposite material for efficient photocatalytic degradation of organic dyes.

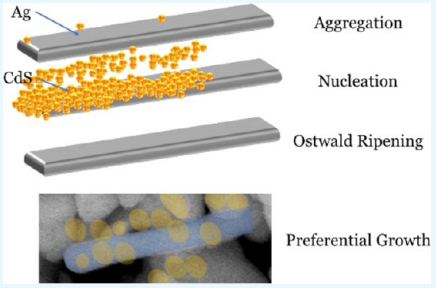

1. INTRODUCTION

Semiconductor materials display abundant consideration toward photocatalytic applications because of their ability to earn the benefit of renewable solar energy to overcome energy difficulties and related environmental issues.[1−10] Photocatalysis, in particular, is considered one of the clean technologies that have been used in a variety of medical and environmental applications. The critical component in photocatalytic reactions that absorb light energy and transform it into chemical reactions is semiconducting photocatalyst materials. This is due to the nanocomposite photocatalysts' improved charge isolation, irradiation absorption, and photo and chemical stability. Nanocomposite materials are frequently used in the field of photocatalysis. Because photocatalysts have different band gap widths and band positions, the electron and hole pairs formed have different oxidation and reduction potentials. However, there are several intractable issues with nanocomposites, such as a lack of effective photocatalytic units and a short lifetime of photogenerated carriers that prevent their widespread use. Therefore, the investigation of altering or decorating nanocomposites via architecture methodologies for improved photocatalytic performance is crucial, but it is fraught with difficulty and obstacles.[7−9] The preparation of various promising nanocomposite photocatalysts can be used to create a practical photocatalyst pathway. For improving the separation of

Scheme 1. Suggested Mechanism for the Development of the Ag-CdSe/GO@CA Nanocomposite Fiber Materials[a]

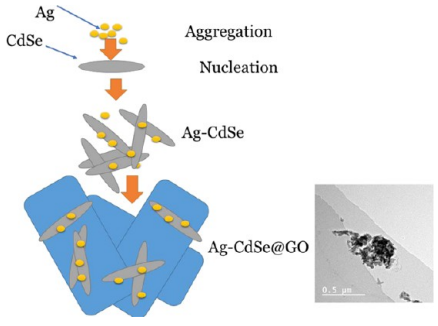

[a]The scale bar is 100 nm.

Received: May 21, 2021
Accepted: July 26, 2021
Published: August 29, 2021

electron−hole pairs and increasing the photocatalytic reaction rate, a variety of advanced materials and approaches have been proposed.[2−8]

Cadmium selenide (CdSe), as inorganic n-type semiconductor nanoparticles, is considered a visible-light-motivated photocatalyst material with a 1.74 eV band gap, reducing organic pollutants in wastewater via photocatalytic behavior that derives from the separation between the photogenerated carriers while irradiated with light.[11−15] Thus, CdSe−based materials have been settled to maximize the nanoparticle photoactive properties.[16−18] One of the possible ways to develop the photocatalytic activity is by doping using different materials, including noble metals (e.g., Ag, Au, Pd, and Pt) as well as carbon-based materials (e.g., graphene, graphene oxide (GO), reduced GO) to form heterostructures for efficiently detaching photogenerated carriers.[19−23] Silver (Ag) as a noble metal has been applied extensively to formulate hybrid metal/semiconductor nanostructures to boost the carrier-separation efficiency.[24−27] In addition, GO characteristics, as carbon-based material with a large surface area, extended π-electron conjugation, and high electron conductivity, make it a promising material for combining with the CdSe semiconductor photocatalyst for supporting the electron−hole separation process.[28−30] Furthermore, cellulose nanofibrous membranes with a tailorable pore size can blend some particulates to achieve the operative separation of dyes and wastewater purification. In addition, the loading of the synthesized semiconductor materials in the cellulose nanofiber membrane networks through electrospinning allows for increasing the contact area and improve wastewater treatment applications.

CdSe is considered a significant photoelectric material because of its auspicious features, including detached energy levels, appropriate band gap, and considerable photoresistivity.[12] The different applications of CdSe, together with its electrical, optical, luminescence, and photo-electronics properties, can be enhanced via doping with heterovalent impurities such as Ag metals along with GO materials.[31−34] CdSe doped with Ag and GO can show improved charge-carrier characteristics that can be taken as an advantage in photocatalytic applications. In this study, we prepared a composite material containing Ag, CdSe, and GO nanomaterials loaded on cellulose acetate (CA) nanofiber membranes as a photocatalyst for the dye removal process.

Herein, we describe the mixture between CdSe nanoparticles with both Ag nanoparticles and GO materials to prepare ternary hybrids composed of Ag-CdSe/GO heterostructural composites. The material was prepared via a solvothermal technique to synthesize uniform CdSe nanoparticles, followed consecutively by incorporating GO and the decoration of Ag by thermal reduction and photodeposition, respectively (Scheme 1). After that, the synthesized composite was loaded onto CA nanofiber membranes and used as a photocatalyst for the dye removal process. The development mechanism of Ag-CdSe/GO@CA composites was anticipated via different characterization techniques. In addition, the photocatalytic activity of Ag-CdSe/GO@CA composites was estimated through the degradation of malachite green (MG) under visible-light irradiation. The findings in this study prove that the semiconductor-based hybrid nanocomposite material is better than the single-component ones and demonstrate the improved charge-separation efficiency, strong redox capability, and long-term stability for efficient photocatalytic degradation of organic dyes.

2. RESULTS AND DISCUSSION

2.1. Analysis of CdSe, Ag-CdSe, CdSe/GO, and Ag-CdSe/GO Nanocomposite Powders. The X-ray diffraction (XRD) patterns of the different CdSe, Ag-CdSe, CdSe/GO, and Ag-CdSe/GO nanocomposite powders and the corresponding materials loaded in CA nanofiber membranes (CdSe@CA, Ag-CdSe@CA, CdSe/GO@CA, and Ag-CdSe/GO@CA) are shown in Figures 1 and 4 to identify the possible phases of the synthesized materials. It is shown that the crystal phase of CdSe particles is wurtzite with a lattice constant of 6.077 Å (JCPDS 19-0191) for cubic structures and ICDD no. 00-008-0459 for the hexagonal symmetry.[31−33] CdSe doped with Ag and GO allows for obtaining Ag-CdSe, CdSe/GO, and Ag-CdSe/GO nanocomposite powders, the diffraction peaks being indexed to a mixture of hexagonal wurtzite CdSe and the face-centered-cubic (fcc) metallic Ag nanoparticles or crystal planes of GO. The change in the diffraction peaks between bare CdSe and the doped samples emphasizes that the prepared nanocomposite materials are formed from the mixture of CdSe and Ag or GO elements (Figure 1). The prominent peak obtained at around 2θ = 11° in Ag-CdSe, CdSe/GO, and Ag-CdSe/GO nanocomposite powders with almost the same XRD peaks can be a consequence of the low loading and/or identical distribution of GO and Ag in the nanocomposite structure.[32,33]

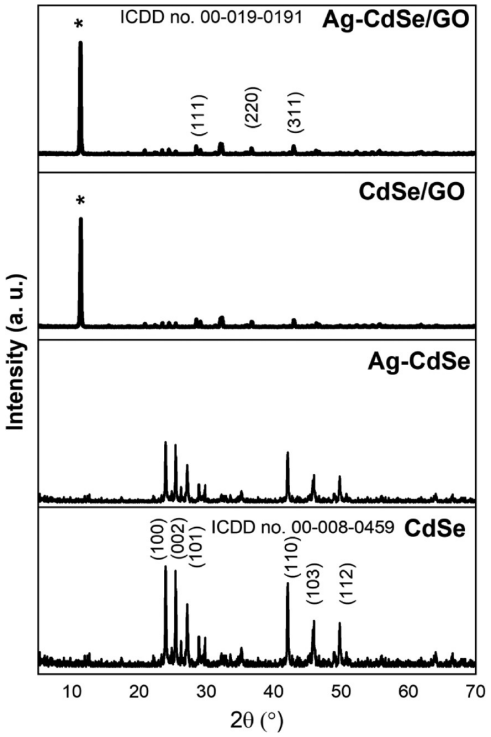

Figure 1. XRD patterns of CdSe, Ag-CdSe, CdSe/GO, and Ag-CdSe/GO nanocomposite powders (*: GO).

The sharp peaks of the obtained CdSe and its derivatives are accompanied by the high crystallinity of the formed compositions, which is assigned to the high temperature through the synthesis process. Furthermore, it could be mentioned that for modified CdSe, there is a sharp peak around 2θ = 11°, which could be assigned to GO. Furthermore, the obvious change in the XRD patterns from Ag-CdSe and CdSe/GO is assigned to the crystallographic transformation of CdSe from hexagonal symmetry into the cubic one. In other words,

https://doi.org/10.1021/acsomega.1c02667
ACS Omega 2021, 6, 23129−23138

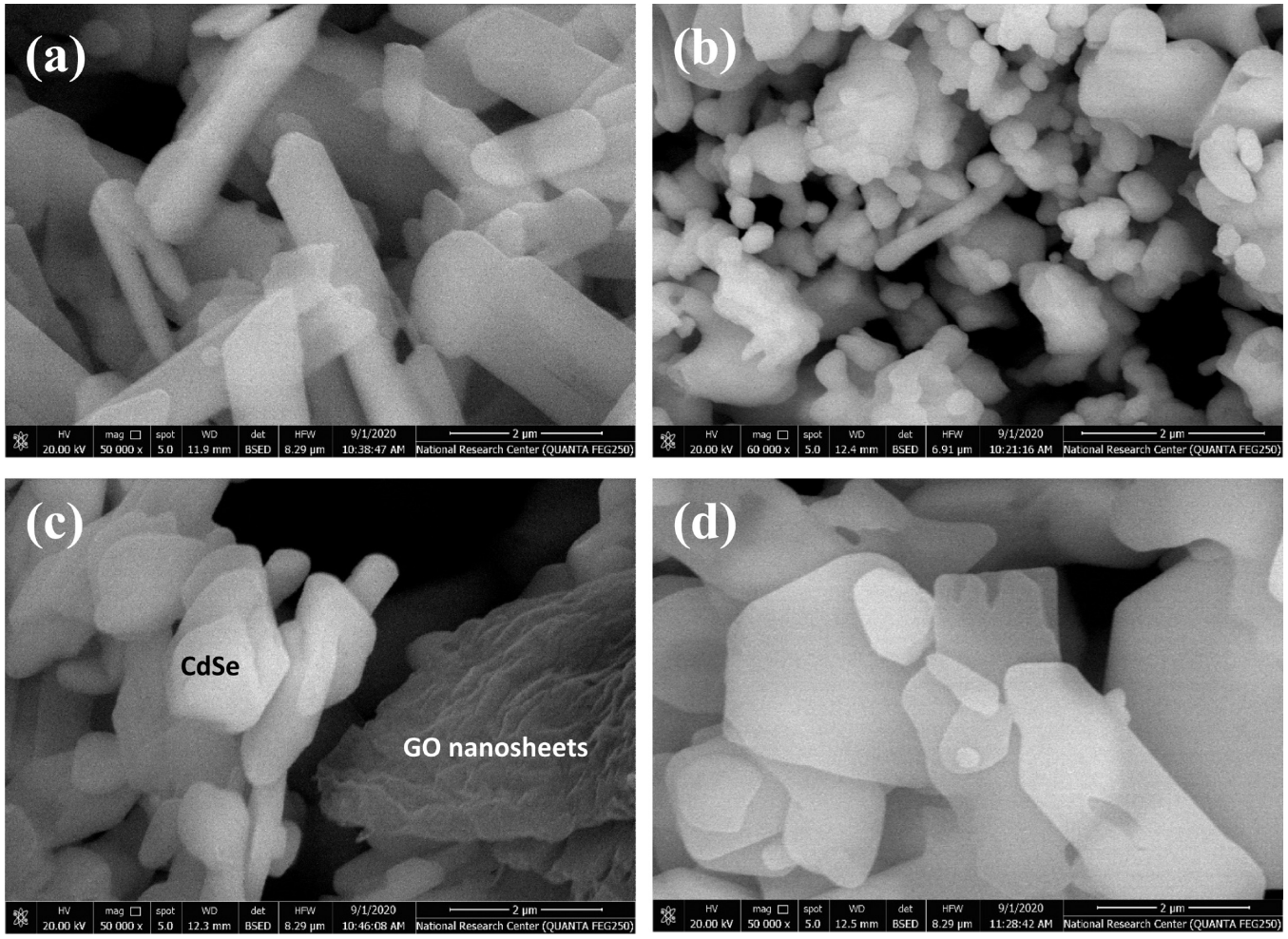

Figure 2. FESEM images of (a) CdSe, (b) Ag-CdSe, (c) CdSe/GO, and (d) Ag-CdSe/GO nanocomposite powders.

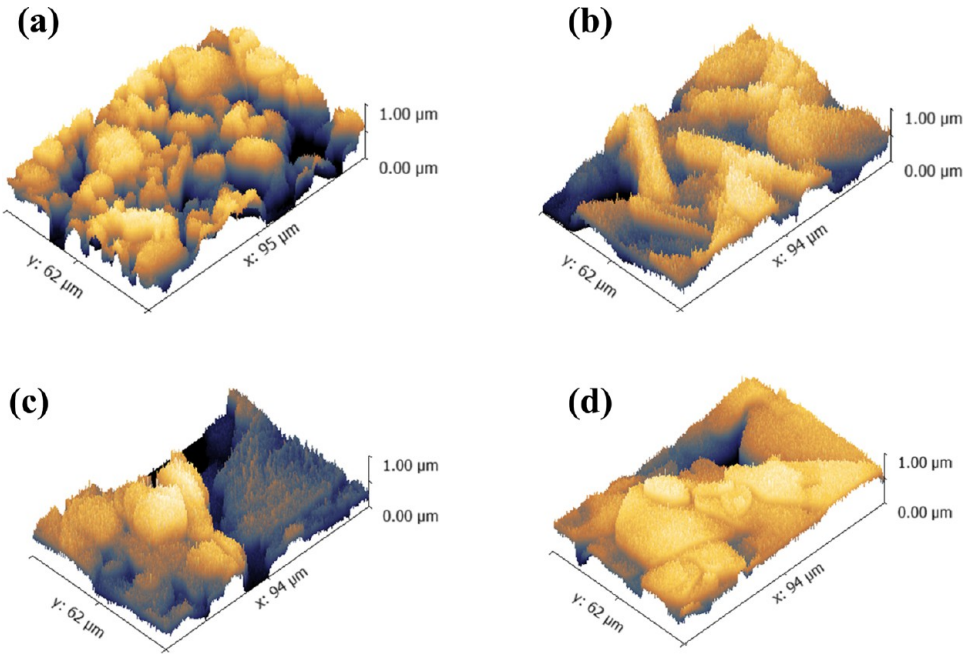

Figure 3. AFM surface images of (a) CdSe, (b) Ag-CdSe, (c) CdSe/GO, and (d) Ag-CdSe/GO nanocomposite powders.

CdSe and Ag-CdSe are formed in a hexagonal symmetry, following the ICDD card no. 00-008-0459, while CdSe and Ag-CdSe/GO are formed in a cubic symmetry, following the ICDD no. 00-019-0191.

https://doi.org/10.1021/acsomega.1c02667
ACS Omega 2021, 6, 23129−23138

Table 1. Roughness Parameters of CdSe, Ag-CdSe, CdSe/GO, and Ag-CdSe/GO Nanocomposite Powders

composition	roughness average (R_a) (nm)	root-mean-square roughness (R_q) (nm)	maximum height of the roughness (R_t) (nm)	maximum roughness valley depth (R_v) (nm)	maximum roughness peak height (R_p) (nm)	average maximum height of the roughness (R_{tm}) (nm)
CdSe	25	33	233	114	119	181
Ag-CdSe	29	38	349	165	185	245
CdSe@GO	27	35	282	136	146	195
Ag-CdSe@GO	36	46	384	177	206	259

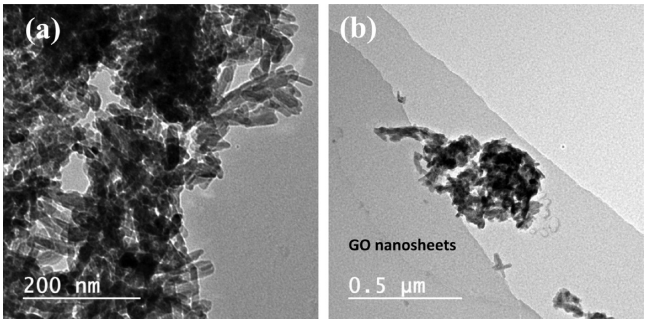

Figure 4. TEM micrographs of (a) Ag-CdSe and (b) Ag-CdSe/GO powder compositions.

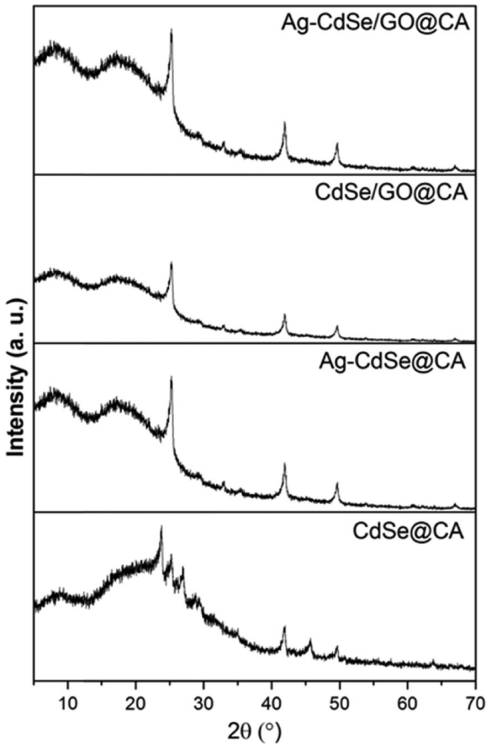

Figure 5. XRD patterns of CdSe, Ag-CdSe, CdSe/GO, and Ag-CdSe/GO nanocomposite powder materials loaded in CA nanofiber membranes (CdSe@CA, Ag-CdSe@CA, CdSe/GO@CA, and Ag-CdSe/GO@CA).

Figure 2a–d shows representative field emission scanning electron microscopy (FESEM) images of the as-synthesized photocatalyst powder materials. The morphology of CdSe nanoparticles shows uniform hexagonal shape wurtzite structure aggregations with different sizes (Figure 2a). Combining a low quantity of Ag and CdSe to form Ag-CdSe nanoparticles is displayed as a mixture of hexagonal wurtzite CdSe and fcc metallic Ag nanoparticles (Figure 2b). Ag nanoparticles with a small amount and small crystallite sizes are responsible for creating nucleation sites for the growth of CdSe clusters, which is essential in lessening the nucleation hurdle to yield the Ag-CdSe nanoparticles.[34] Furthermore, the addition of the CdSe nanoparticles to GO shows nonvarying shape morphology of the CdSe nanoparticles with uniform distribution on the surface of GO, establishing thick heterostructure active sites on the smooth surface (Figure 2c). The amalgamation of the Ag-CdSe nanoparticles to the GO matrix to form Ag-CdSe/GO nanocomposite powders shows almost no alteration in the morphology of the Ag-CdSe nanoparticles. The Ag-CdSe nanoparticles attach firmly to the surface of the GO nanosheets (Figure 2d). The contact between the Ag-CdSe nanoparticles and GO matrix can facilitate the electron transfer from CdSe nanoparticles to Ag and/or GO, which can support photogenerated electron–hole pair separation.[35]

Topographic morphology images of the prepared CdSe, Ag-CdSe, CdSe/GO, and Ag-CdSe/GO nanocomposite powders were obtained by three-dimensional (3D) atomic force microscopy (AFM) measurements, as presented in Figure 3a–d. Various consistently sized CdSe nanoparticles are detected with the homogeneous distribution of the particles (Figure 3a).[36,37] After the addition of Ag nanoparticles and/or GO materials, there is no noticeable change detected for the particle distribution, except for some dark parts in the case of the CdSe/GO nanocomposite materials, illustrating the presence of the GO matrix in the structure (Figure 3b,c). In the case of Ag-CdSe/GO nanocomposite powders (Figure 3d), the AFM data display an excellent attachment of Ag-CdSe with the GO nanosheets and demonstrate a uniform distribution on the surface, which can be favorable to progress the efficiency of the photocatalyst materials. In addition, the synthesized materials revealed a roughness average of 25, 29, 27, and 36 and root-mean-square roughness of 33, 38, 35, and 46, while the average maximum heights of the roughness [(R_{tm}): (nm)] are 181, 245, 195, and 259 for CdSe, Ag-CdSe, CdSe/GO, and Ag-CdSe/GO nanocomposite powders, respectively. In addition, Table 1 shows the roughness parameters for the prepared CdSe, Ag-CdSe, CdSe/GO, and Ag-CdSe/GO nanocomposite powders, as well as the roughness average, root-mean-square roughness, maximum roughness valley width, maximum roughness peak height, and average maximum height of the roughness.

2.2. Microstructural Features. Transmission electron microscopy (TEM) micrographs show that the modified CdSe with Ag ions has been formed in an elongated shape with lengths in the range of 35–70 nm, as shown in Figure 4a. In addition, the nanoparticles seem to be agglomerated, while their distribution tends to be homogeneous. Furthermore, the incorporation of Ag-CdSe through GO nanosheets is illustrated in Figure 4b. The nanoparticles are sandwiched by GO sheets, which appear in microdimensions. The encapsulation of modified CdSe nanoparticles through GO plays a significant role in delivering photogenerated electrons between CdSe and GO, decreasing the probability of recombination and thus promoting electrical

https://doi.org/10.1021/acsomega.1c02667
ACS Omega 2021, 6, 23129–23138

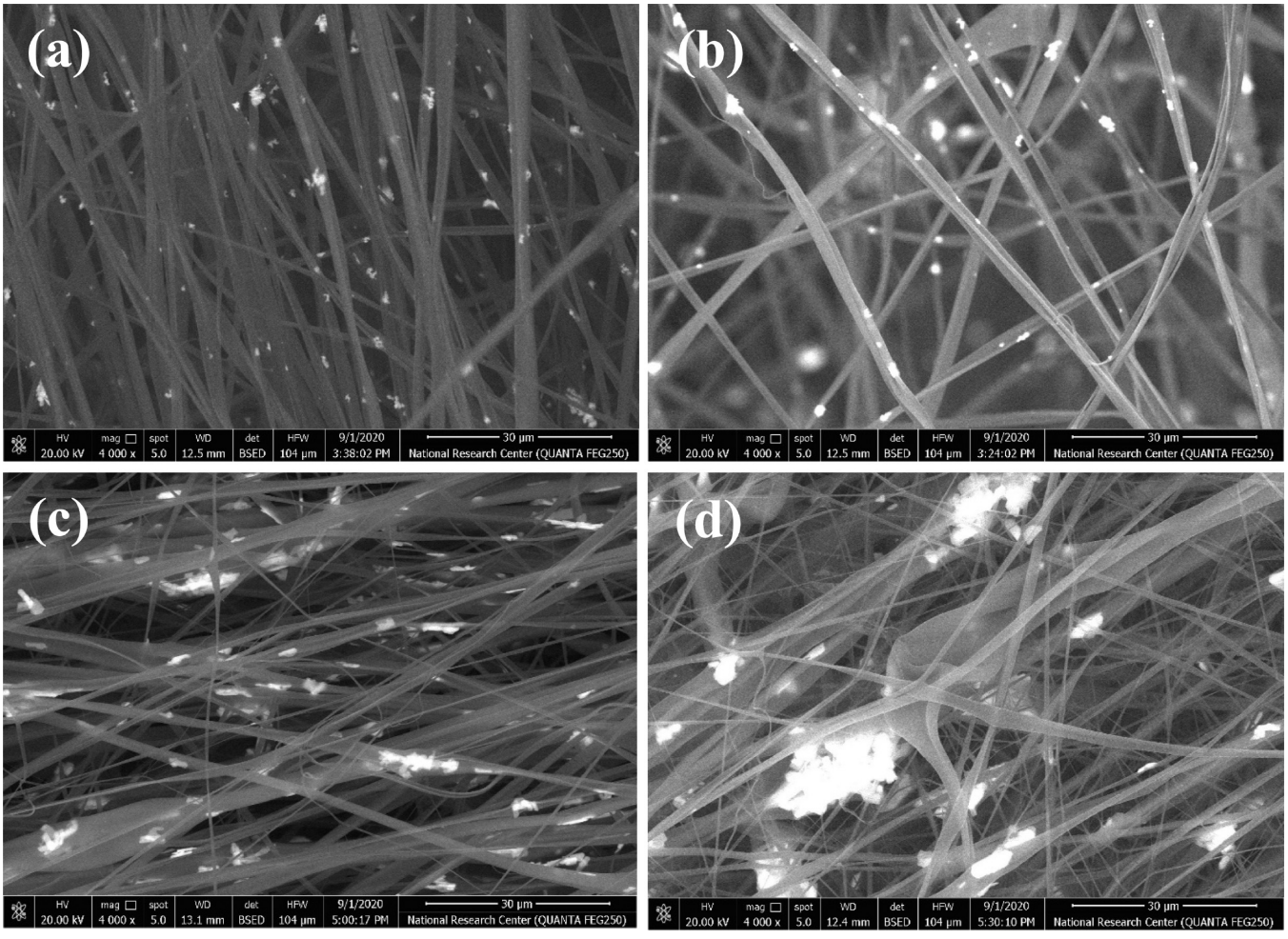

Figure 6. FESEM images of (a) CdSe@CA, (b) Ag-CdSe@CA, (c) CdSe/GO@CA, and (d) Ag-CdSe/GO@CA nanocomposite fibers.

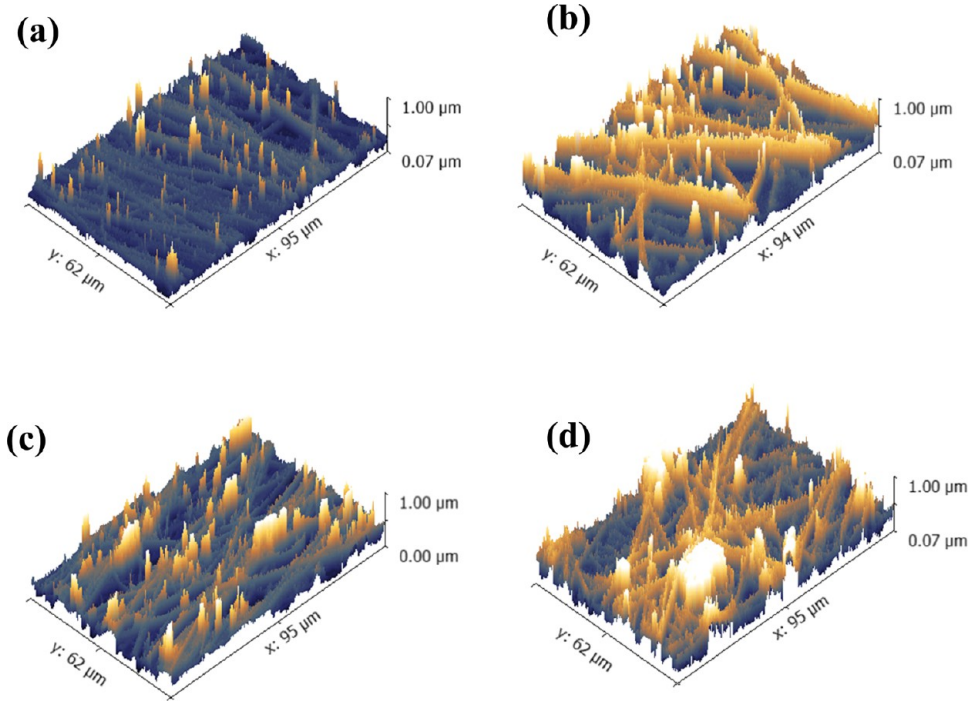

Figure 7. 3D AFM images of (a) CdSe@CA, (b) Ag-CdSe@CA, (c) CdSe/GO@CA, and (d) Ag-CdSe/GO@CA nanocomposite fibers.

https://doi.org/10.1021/acsomega.1c02667
ACS Omega 2021, 6, 23129−23138

Table 2. Roughness Parameters of CdSe@CA, Ag-CdSe@CA, CdSe/GO@CA, and Ag-CdSe/GO@CA Nanocomposite Fibers

composition	R_a (nm)	R_q (nm)	R_t (nm)	R_v (nm)	R_p (nm)	R_{tm} (nm)
CdSe@CA	29	40	332	155	176	278
Ag-CdSe@CA	29	40	489	276	213	269
CdSe/GO@CA	34	46	512	223	289	327
Ag-CdSe/GO@CA	35	48	461	265	195	283

Scheme 2. Representation Chart Demonstrating the Degradation Mechanism of MG over Ag-CdSe/GO@CA Nanocomposite Fiber Samples

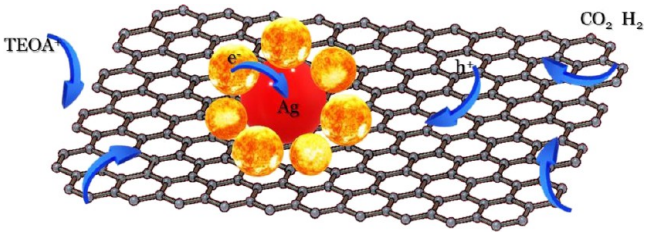

conductivity. This scenario is essential for photoelectric-based applications.

2.3. Analysis of CdSe@CA, Ag-CdSe@CA, CdSe/GO@CA, and Ag-CdSe/GO@CA Nanocomposite Fibers. Furthermore, the different as-prepared powders were loaded in CA nanofiber membranes to form CdSe@CA, Ag-CdSe@CA, CdSe/GO@CA, and Ag-CdSe/GO@CA nanocomposite fibers. XRD confirmed the crystal structure of the synthesized fibers, and the data display the coexistence of the amorphous structure of CA with a broad peak at $2\theta = 22°$, with the other different peaks related to CdSe, as well as the mixture of CdSe with Ag and GO (Figure 5). The same is found in the nanocomposite fibers that show nearly similar XRD peaks in all-fiber samples, indicating the distribution of GO through the nanocomposite structure.[33]

Subsequently, after the preparation of CdSe, Ag-CdSe, CdSe/GO, and Ag-CdSe/GO nanocomposite powders, the materials were led in CA to form CdSe@CA, Ag-CdSe@CA, CdSe/GO@CA, and Ag-CdSe/GO@CA nanocomposite fibers for photocatalytic applications. The microstructure and surface morphologies of the different prepared fiber materials were evaluated using FESEM images, as presented in Figure 6a−d. The CdSe particles were loaded in CA nanofiber membranes to form CdSe@CA randomly oriented nanofibers, with an average diameter of about 450−650 nm and a smooth surface (Figure 6a). For Ag-CdSe and/or CdSe/GO composites loaded in CA, both the Ag nanoparticles and GO materials preserve the linear structures of the obtained fibers, and the outer CdS partials have sizes from 100 to 200 nm (Figure 6b,c). Similarly, the addition of the synthesized Ag-CdSe/GO nanocomposites to the CA nanofibers leads to Ag-CdSe/GO@CA nanocomposite fibers displaying a similar fiber morphology (Figure 6d).

The equivalent topographic morphologies for the prepared CdSe@CA, Ag-CdSe@CA, CdSe/GO@CA, and Ag-CdSe/GO@CA nanocomposite fibers were evaluated by 3D AFM measurements (Figure 7a−d). The topography of the samples seems to be almost the same with relatively low variations, illustrating the homogeneous distribution of the fibers and the attachment between the powder materials with the CA nanofiber matrix membrane. In addition, the roughness average values of the prepared fiber materials are 29, 29, 34, and 35 nm and the root-mean-square roughness values are 40, 40, 46, and 48, while the average maximum heights of the roughness are 278, 269, 327, and 283 for CdSe@CA, Ag-CdSe@CA, CdSe/GO@CA, and Ag-CdSe/GO@CA nanocomposite fibers, respectively. The roughness parameters for the prepared nanocomposite fibers are summarized in Table 2. The development of roughness parameters upon the change of compositions is assigned to the crystallographic defects accompanied by the ionic dopants. Moreover, increasing roughness parameters facilitates physical adhesion with the surrounding and promotes interlocking mechanisms between the membranes and the ambient atmosphere. Thus, chemical interactions among nanofibrous membranes and neighbored molecules might be progressed upon the increase in roughness.

Stress−strain measurements appraised the tensile mechanical properties. In addition, the stress−strain characteristic curves of CdSe@CA, Ag-CdSe@CA, CdSe/GO@CA, and Ag-CdSe/GO@CA nanocomposite fibers indicate that the mechanical performance, as well as the tensile strength, improved remarkably in the sequence of CdSe@CA > Ag-CdSe@CA > CdSe/GO@CA > Ag-CdSe/GO@CA after 30%, as shown in Figure S1, in the Supporting Information. The findings show that combining different prepared materials with long chains of CA nanofiber membranes can improve the flexibility and mechanical strength of nanocomposite fibers, allowing them to be used as effective photocatalyst materials. Table S1, Supporting Information summarizes the mechanical properties of nanofibrous membranes, such as fracture power, tensile strength, maximum strain at break, and toughness, as a function of the composition of CdSe@CA, Ag-CdSe@CA, CdSe/GO@CA, and Ag-CdSe/GO@CA nanocomposite fibers.

2.4. Photocatalytic Performance of Different Nanocomposite Fibers. As a representative of the rest of the developed materials, the photocatalytic performance of the Ag-CdSe/GO nanocomposites as well as the loaded ones in CA (Ag-CdSe/GO@CA) is evaluated via the photocatalytic regression of MG under visible-light irradiation. The photocatalytic reaction of MG is detected through the ultraviolet−visible (UV−vis) spectrum in the presence of the nanocomposite materials. Figure 8a,b demonstrates the absorption photo−removal spectrum of Ag-CdSe/GO and Ag-CdSe/GO@CA, respectively, over MG dye at different illumination time periods. The presence of CA nanofiber membranes indicate the suitable photocatalytic performance of the Ag-CdSe/GO@CA sample as the nanofiber membranes lead to the excrescent spreading of Ag-CdSe/GO on the surface, which could improve the heterojunction structure, resulting in enhanced photocatalytic activity.[38−40]

First-order reaction kinetics allow for describing the chemical kinetics of the photodegradation rates of MG dye for the nanocomposite materials. The corresponding C/C_0 and the $\ln(C/C_0)$ plot show a noticeable linear relationship (Figure 8c,d). The degradation rates of MG are found to be 92, 94, 94, and 97% in the existence of CdSe@CA, Ag-CdSe@CA, CdSe/GO@CA, and Ag-CdSe/GO@CA nanocomposite fibers, respectively (Figure 8c). The results reveal that the Ag-CdSe/GO@CA nanocomposite fibers have significantly improved the degradation efficiency. In addition, the photocatalytic reaction rate constant (K_{app}) of MG dye is established to be 3.17, 3.51, 3.45, and 4.07 with correlation coefficients (R^2) of 0.964, 0.899, 0.988, and 0.944 for CdSe@CA, Ag-CdSe@CA, CdSe/GO@CA, and Ag-CdSe/GO@CA nanocomposite fibers, respectively

https://doi.org/10.1021/acsomega.1c02667
ACS Omega 2021, 6, 23129−23138

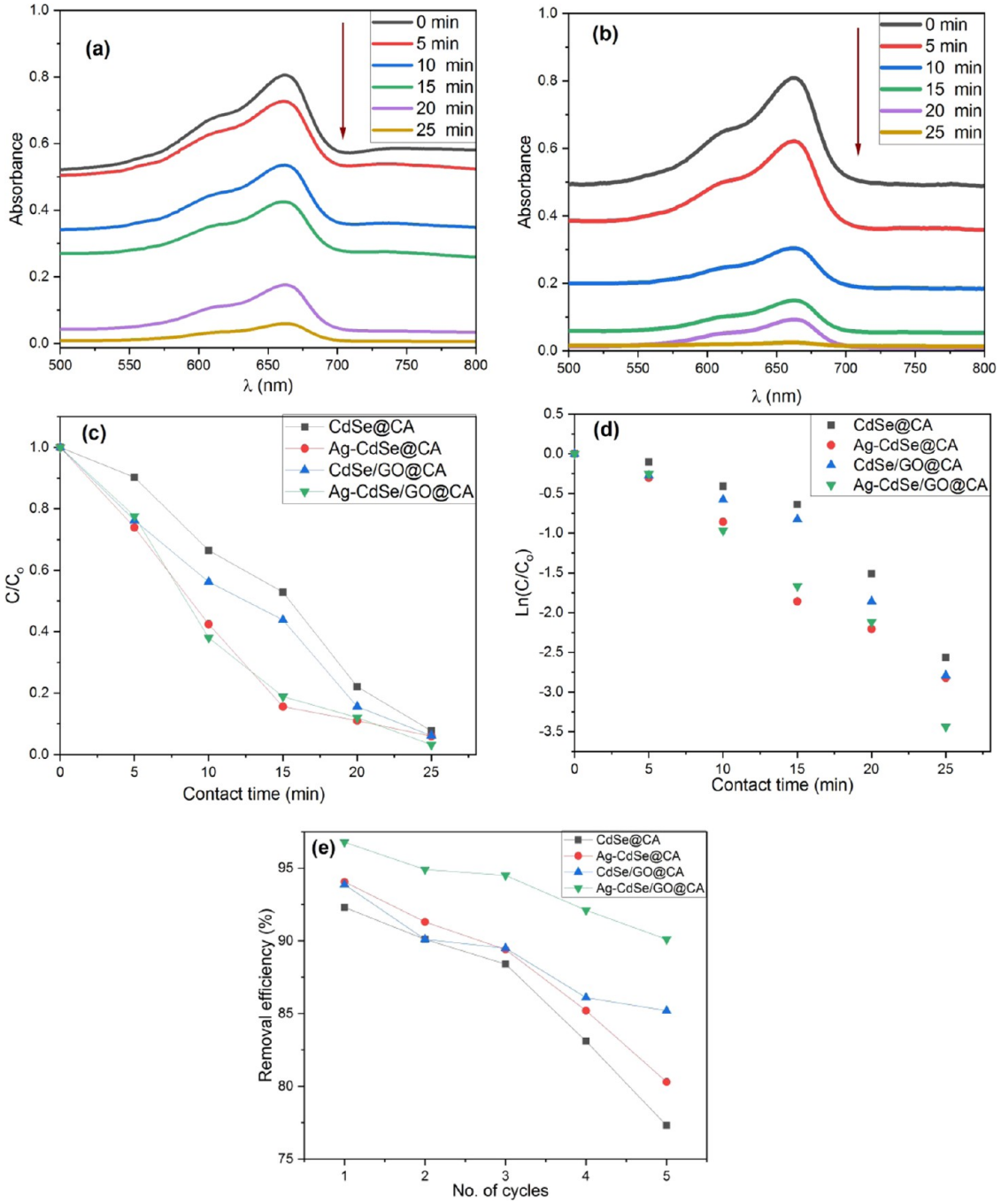

Figure 8. (a, b) Absorption spectrum of the photo−removal of Ag-CdSe/GO and Ag-CdSe/GO@CA over MG dye, (c, d) pseudo-first-order kinetics of the removal of MG, and (e) regeneration of five successive cycles of CdSe@CA, Ag-CdSe@CA, CdSe/GO@CA, and Ag-CdSe/GO@CA nanocomposite fibers.

(Figure 8d). The photocatalytic reaction rate constant of Ag-CdSe/GO@CA has the highest value, indicating that the synergetic influence of Ag-CdSe/GO and CA is beneficial to photocatalytic activity improvements.

The reusability and stability effectiveness of the photocatalyst is an essential factor toward its commercial use and practical applications. The cycling experiment was checked to remove MG dye in the existence of CdSe@CA, Ag-CdSe@CA, CdSe/GO@CA, and Ag-CdSe/GO@CA nanocomposite fibers for five different cycles. Figure 8e proves that Ag-CdSe/GO@CA nanocomposite fibers display a slight decrease in the photocatalytic efficiency during the cycling experiment compared to the other nanocomposite fibers. Consequently, the Ag-CdSe/GO@CA nanocomposite fibers show improved stability and reuse efficiency toward the degradation of MG dye.

Based on the acquired results, we anticipated a conceivable mechanism for photocatalytic degradation of MG over Ag-CdSe/GO@CA nanocomposite fibers (Scheme 2). The electrons are excited under visible-light irradiation from the valence band (VB) of CdSe to its conduction band (CB) to form photogenerated electron−hole pairs. As the CB edge of CdSe is more negative than the Fermi level of GO and Ag, the photogenerated electrons in the CB of CdSe move to Ag and GO. In addition, GO can work as an electron acceptor toward

https://doi.org/10.1021/acsomega.1c02667
ACS Omega 2021, 6, 23129−23138

Table 3. Comparison of Photocatalyst Substances Correlates to Ag-CdSe@CA and Their Conditions for MB under Visible Light

composition	adsorbent conc. (mg/mL)	dye conc. (ppm)	removal eff. (%)	exposure time (min)	ref.
GO	10	18	31.47	210	44
$CuFe_2O_4$	10	18	62.37	210	44
Cu-Fe_2O_4/GO	10	18	90.7	210	44
starch-coated CdSe	30	31	98.3	12.5	45
CdSe/TiO_2	10	10	99	360	46
hexagonal CdSe	100	8	92	50	47
CdSe@CA	120	5	92	25	this work
Ag-CdSe@CA	120	5	94	25	this work
CdSe/GO@CA	120	5	94	25	this work
Ag-CdSe/GO@CA	120	5	97	25	this work

electron transfer from CdSe materials.[41−43] The presence of CA nanofiber membranes facilitates the charge separation and carrier movement, which produce augmentation of the photocatalytic reaction. Consequently, the excited electrons in Ag-CdSe/GO@CA nanocomposite fibers will be surrounded by means of absorbed O_2 to form $O_2^{\cdot-}$. In addition, the hazardous pollutants in wastewater can be oxidized through the collected holes on the surface of Ag-CdSe/GO@CA nanocomposite materials. For this reason, the Ag-CdSe/GO@CA nanocomposite fiber photocatalyst presents outstanding performance toward photodegradation of organic dyes for the wastewater treatment.

As reported in Table 3, G. Han et al. synthesized CdSe with a hexagonal symmetry for MG degradation in aqueous solutions. After 50 min of exposure to visible-light irradiation, 92% of MG was degraded.[47]

3. CONCLUSIONS

CdSe materials, together with the doped Ag-CdSe and Ag-CdSe/GO nanocomposite structures, in addition to the loaded ones on CA nanofiber membranes (CdSe@CA, Ag-CdSe@CA, CdSe/GO@CA, and Ag-CdSe/GO@CA), were prepared. Different characterization techniques together with XRD, FESEM, and AFM disclose the formation of nanocomposite fibers with anticipated properties. CdSe doped with Ag and GO and loaded with CA allow for obtaining different nanocomposite powders with diffraction peaks that are indexed to a mixture of hexagonal wurtzite and fcc structure with good roughness as well as a homogeneous distribution of the fibers with the CA nanofiber matrix membrane. The photocatalysis results confirm that the Ag-CdSe/GO@CA heterostructural composites reveal enhanced photocatalytic activity compared to the other materials loaded in CA nanofiber membranes owing to the charge separation in addition to the subsequent OH radicals. Additionally, the Ag-CdSe/GO@CA nanocomposite fibers express amended stability, and the photocatalytic activity remains virtually unaffected after five recycles. Our study substantiates that the obtained semiconductor-based hybrid nanocomposite materials show improved photocatalytic activity, depending on the charge-separation efficiency, strong redox capability, and long-term stability for efficient photocatalytic degradation of organic dyes. The degradation effectiveness deteriorated with the number of cycles because of the topographical changes that might have occurred from one cycle to another. The hydrophilic behavior of the compositions could deteriorate, which leads to a decrease in reaction probability, thus a lowering of the efficiency.

4. EXPERIMENTAL SECTION

4.1. Synthesis. CdSe modified with Ag ions and GO has been synthesized by means of the hydrothermal process. In brief, for pure CdSe composition, 0.2 M of cadmium chloride and 0.2 M of sodium selenite have been dissolved using double-distilled water individually through 50 mL of distilled water; then, they have been added and introduced into an autoclave of 250 mL for 4 h at a temperature of 120 °C. The obtained solution was then filtered and washed using ethanol and double-distilled water. Then, the precipitated gel was dried via a drier furnace at 50−60 °C. The modified composition of Ag-CdSe was obtained as follows: 0.18 M of cadmium chloride, 0.2 M of sodium selenite, and 0.02 M of silver nitrate solution was prepared and dissolved in double-distilled water to be introduced into the autoclave, as explained previously. Regarding the additional GO compositions, 0.05 g of GO was added for each composition, as mentioned in Table 4, using the following equation:

Table 4. Contributions of Precursors for the Preparation of CdSe Modified with Ag Ions and GO, Together with Its Additions into CA for Nanofiber Phases

composition	$CdCl_2$ (g)	Na_2SeO_3 (g)	$AgNO_3$ (g)	GO (g)	CA (g/mL)
CdSe	3.664	3.458		0.05	
Ag-CdSe	3.299	3.458	0.339	0.05	
CdSe/GO	3.664	3.458		0.05	
Ag-CdSe/GO	3.299	3.458	0.339	0.05	
CdSe@CA	3.664	3.458		0.05	1.0
Ag-CdSe@CA	3.299	3.458	0.339	0.05	1.0
CdSe/GO@CA	3.664	3.458		0.05	1.0
Ag-CdSe/GO@CA	3.299	3.458	0.339	0.05	1.0

$$AgNO_3 + CdCl_2 + Na_2SeO_3 \rightarrow Ag - CdSe + 2NaCl \quad (1)$$

To produce the nanofibrous membranes, the obtained powders then were treated with CA as follows: 110 mg of each powder sample was added to a CA solution (10 wt %) dissolved in acetone to be introduced into a syringe pump for membrane preparation by electrospinning. The electrospinning was carried out at a high voltage of 18 kV, with a 1 mL/h injection rate and a needle-to-collector distance of 16 cm.

4.2. Characterization. XRD analyses were accompanied to categorize the phase composition by means of monochromatized Cu kα radiation (λ = 1.5404 Å) at 40 kV with a step size 0.02° and 0.5 s. The surface morphology of the particles and membranes was considered by FESEM (QUANTA-FEG250, Netherlands). At this point, the obtained graphs have been processed with the Gwyddion 2.45 software to study the surface roughness. Mechanical tests were carried out on nanofibrous samples using a tensile-compressive tester (LR10K, LLOYD, USA). Experiments were performed with a 5 mm/min deformation rate up to the breaking point, following the ASTM D882 standard.

4.3. Photocatalytic Setup. The photocatalytic properties of CdSe and its modifications were investigated using the MG dye as a model. The starting concentration of MG solution in

https://doi.org/10.1021/acsomega.1c02667
ACS Omega 2021, 6, 23129−23138

water is 5 mg/L, while the CdSe nanofiber dosage is 120 mg. In order to do so, 120 mg of the matrix (roughly 1.3 x 1.3 cm) was introduced into a beaker containing 5 mg/L of MG in a total volume of 30 mL. To obtain well-dispersed solutions, ultrasonication was used. The irradiation source was obtained from a 300 W mercury lamp light source (the distance is 15 cm). Before being exposed to irradiation, the samples were dyed without being exposed to irradiation in order to test the dye's efficacy in the dark. Using a double beam spectrophotometer (Shimadzu UV-1208 model) and the following expression, the performance (η %) was calculated spectrophotometrically:

$$\eta(\%) = \left(\frac{C_0 - C_t}{C_0}\right) \times 100 \quad (2)$$

where C_o and C_t are the initial concentration and the concentration at the irradiation time (t).

■ ASSOCIATED CONTENT

Supporting Information

The Supporting Information is available free of charge at https://pubs.acs.org/doi/10.1021/acsomega.1c02667.

Tensile stress−strain curves and mechanical properties of nanofibrous membranes, including fracture strength, tensile strength, maximum strain at break, and toughness upon the composition of CdSe@CA, Ag-CdSe@CA, CdSe/GO@CA, and Ag-CdSe/GO@CA nanocomposite fibers (PDF)

■ AUTHOR INFORMATION

Corresponding Authors

Mohamed K. Ahmed − *Department of Physics, Faculty of Science, Suez University, Suez 43518, Egypt; Academy of Scientific Research and Technology (ASRT), Cairo 11516, Egypt; Faculty of Nanotechnology for Postgraduate Studies, Cairo University, El-Sheikh Zayed 12588, Egypt*; Email: m.khalaf@sci.suezuni.edu.eg

Ahmed Esmail Shalan − *Central Metallurgical Research and Development Institute (CMRDI), Helwan, Cairo 11421, Egypt; BCMaterials, Basque Center for Materials, Applications and Nanostructures, Martina Casiano, UPV/EHU Science Park, Leioa 48940, Spain*; orcid.org/0000-0002-3424-1609; Email: a.shalan133@gmail.com, ahmed.shalan@bcmaterials.net

Mohamed Afifi − *Faculty of Nanotechnology for Postgraduate Studies, Cairo University, El-Sheikh Zayed 12588, Egypt; Ultrasonic Laboratory, National Institute of Standards, Giza 12211, Egypt*; Email: mahmoud@daad-alumni.de, phafifi@gmail.com

Mohamed M. El-Desoky − *Department of Physics, Faculty of Science, Suez University, Suez 43518, Egypt; Academy of Scientific Research and Technology (ASRT), Cairo 11516, Egypt*; Email: mmdesoky@suezuniv.edu.eg

Senentxu Lanceros-Méndez − *BCMaterials, Basque Center for Materials, Applications and Nanostructures, Martina Casiano, UPV/EHU Science Park, Leioa 48940, Spain; IKERBASQUE, Basque Foundation for Science, 48009 Bilbao, Spain*; Email: senentxu.lanceros@bcmaterials.net

Complete contact information is available at: https://pubs.acs.org/10.1021/acsomega.1c02667

Notes

The authors declare no competing financial interest.

■ ACKNOWLEDGMENTS

The Academy of Scientific Research and Technology (ASRT), Egypt, Grant No. 6510, supported this project financially.

■ REFERENCES

(1) Chen, Z.; Liu, S.; Yang, M.-Q.; Xu, Y.-J. Synthesis of Uniform CdS Nanospheres/Graphene Hybrid Nanocomposites and Their Application as Visible Light Photocatalyst for Selective Reduction of Nitro Organics in Water. *ACS Appl. Mater. Interfaces* **2013**, *5*, 4309−4319.

(2) El-Shazly, A. N.; Rashad, M. M.; Abdel-Aal, E. A.; Ibrahim, I. A.; El-Shahat, M. F.; Shalan, A. E. Nanostructured ZnO Photocatalysts Prepared via Surfactant Assisted Co-Precipitation Method Achieving Enhanced Photocatalytic Activity for the Degradation of Methylene Blue Dyes. *J. Environ. Chem. Eng.* **2016**, *4*, 3177−3184.

(3) Khanchandani, S.; Kundu, S.; Patra, A.; Ganguli, A. K. Shell Thickness Dependent Photocatalytic Properties of ZnO/CdS Core−Shell Nanorods. *J. Phys. Chem. C* **2012**, *116*, 23653−23662.

(4) Taheri-Ledari, R.; Esmaeili, M. S.; Varzi, Z.; Eivazzadeh-Keihan, R.; Maleki, A.; Shalan, A. E. Facile Route to Synthesize Fe_3O_4@acacia−SO_3H Nanocomposite as a Heterogeneous Magnetic System for Catalytic Applications. *RSC Adv.* **2020**, *10*, 40055−40067.

(5) Taheri-Ledari, R.; Rahimi, J.; Maleki, A.; Shalan, A. E. Ultrasound-Assisted Diversion of Nitrobenzene Derivatives to Their Aniline Equivalents through a Heterogeneous Magnetic Ag/Fe_3O_4-IT Nanocomposite Catalyst. *New J. Chem.* **2020**, *44*, 19827−19835.

(6) Abdelbasir, S. M.; Shalan, A. E. An Overview of Nanomaterials for Industrial Wastewater Treatment. *Korean J. Chem. Eng.* **2019**, *36*, 1209−1225.

(7) Sanad, M. F.; Abu Serea, E. S.; Bazid, S. M.; Nabih, S.; Ahsan, M. A.; Shalan, A. E. High Cytotoxic Activity of ZnO@leucovorin Nanocomposite Based Materials against an MCF-7 Cell Model. *Anal. Methods* **2020**, *12*, 2176−2184.

(8) Fahmy, H. M.; Mosleh, A. M.; Elghany, A. A.; Shams-Eldin, E.; Abu Serea, E. S.; Ali, S. A.; Shalan, A. E. Coated Silver Nanoparticles: Synthesis, Cytotoxicity, and Optical Properties. *RSC Adv.* **2019**, *9*, 20118−20136.

(9) Wang, Y.-C.; Liu, X.-Y.; Wang, X.-X.; Cao, M.-S. Metal-Organic Frameworks Based Photocatalysts: Architecture Strategies for Efficient Solar Energy Conversion. *Chem. Eng. J.* **2021**, *419*, No. 129459.

(10) Rashad, M. M.; Elsayed, E. M.; Al-Kotb, M. S.; Shalan, A. E. The Structural, Optical, Magnetic and Photocatalytic Properties of Transition Metal Ions Doped TiO_2 Nanoparticles. *J. Alloys Compd.* **2013**, *581*, 71−78.

(11) Qu, L.; Peng, X. Control of Photoluminescence Properties of CdSe Nanocrystals in Growth. *J. Am. Chem. Soc.* **2002**, *124*, 2049−2055.

(12) Myung, N.; Ding, Z.; Bard, A. J. Electrogenerated Chemiluminescence of CdSe Nanocrystals. *Nano Lett.* **2002**, *2*, 1315−1319.

(13) Shu, G.-W.; Lee, W.-Z.; Shu, I.-J.; Shen, J.-L.; Lin, J. C.-A.; Chang, W. H.; Ruaan, R.-C.; Chou, W. C. Photoluminescence of Colloidal CdSe/ZnS Quantum Dots under Oxygen Atmosphere. *IEEE Trans. Nanotechnol.* **2005**, *4*, 632−636.

(14) Groeneveld, E.; Witteman, L.; Lefferts, M.; Ke, X.; Bals, S.; Van Tendeloo, G.; de Mello Donega, C. Tailoring ZnSe−CdSe Colloidal Quantum Dots via Cation Exchange: From Core/Shell to Alloy Nanocrystals. *ACS Nano* **2013**, *7*, 7913−7930.

(15) Sahu, A.; Kang, M. S.; Kompch, A.; Notthoff, C.; Wills, A. W.; Deng, D.; Winterer, M.; Frisbie, C. D.; Norris, D. J. Electronic Impurity Doping in CdSe Nanocrystals. *Nano Lett.* **2012**, *12*, 2587−2594.

(16) Soloviev, V. N.; Eichhöfer, A.; Fenske, D.; Banin, U. Size-Dependent Optical Spectroscopy of a Homologous Series of CdSe Cluster Molecules. *J. Am. Chem. Soc.* **2001**, *123*, 2354−2364.

(17) Qu, L.; Peng, Z. A.; Peng, X. Alternative Routes toward High Quality CdSe Nanocrystals. *Nano Lett.* **2001**, *1*, 333−337.

(18) Troparevsky, M. C.; Kronik, L.; Chelikowsky, J. R. Optical Properties of CdSe Quantum Dots. *J. Chem. Phys.* **2003**, *119*, 2284−2287.
(19) Chen, W.-T.; Yang, T.-T.; Hsu, Y.-J. Au-CdS Core−Shell Nanocrystals with Controllable Shell Thickness and Photoinduced Charge Separation Property. *Chem. Mater.* **2008**, *20*, 7204−7206.
(20) Fang, J.; Xu, L.; Zhang, Z.; Yuan, Y.; Cao, S.; Wang, Z.; Yin, L.; Liao, Y.; Xue, C. Au@TiO_2−CdS Ternary Nanostructures for Efficient Visible-Light-Driven Hydrogen Generation. *ACS Appl. Mater. Interfaces* **2013**, *5*, 8088−8092.
(21) Viana, M. M.; Mohallem, N. D. S.; Miquita, D. R.; Balzuweit, K.; Silva-Pinto, E. Preparation of Amorphous and Crystalline Ag/TiO_2 Nanocomposite Thin Films. *Appl. Surf. Sci.* **2013**, *265*, 130−136.
(22) Yang, T.-T.; Chen, W.-T.; Hsu, Y.-J.; Wei, K.-H.; Lin, T.-Y.; Lin, T.-W. Interfacial Charge Carrier Dynamics in Core−Shell Au-CdS Nanocrystals. *J. Phys. Chem. C* **2010**, *114*, 11414−11420.
(23) Zhang, N.; Liu, S.; Fu, X.; Xu, Y.-J. Fabrication of Coenocytic Pd@CdS Nanocomposite as a Visible Light Photocatalyst for Selective Transformation under Mild Conditions. *J. Mater. Chem.* **2012**, *22*, 5042.
(24) Liu, Y.; Chi, M.; Dong, H.; Jia, H.; Xu, B.; Zhang, Z. Ag/CdS Heterostructural Composites: Fabrication, Characterizations and Photocatalysis. *Appl. Surf. Sci.* **2014**, *313*, 558−562.
(25) Zhao, F. A.; Xiao, H. Y.; Bai, X. M.; Zu, X. T. Effects of Ag Doping on the Electronic and Optical Properties of CdSe Quantum Dots. *Phys. Chem. Chem. Phys.* **2019**, *21*, 16108−16119.
(26) Ma, C.; Yao, X.; Wang, L.; Cai, Z.; Huang, H.; Gao, X.; Chen, R.; Liu, Y.; Huo, P.; Yan, Y. Synthesis of Ag Nanoparticles as Cocatalyst onto CdSe/Al_2TiO_5 Composite Photocatalysts for Enhancing Photocatalytic Activity. *J. Environ. Chem. Eng.* **2018**, *6*, 686−693.
(27) Sreejith, K.; Nuwad, J.; Thinaharan, C.; Dey, G. K.; Pillai, C. G. S. Ag Nanoparticle Mediated Growth of CdS Nanobelts. *Appl. Surf. Sci.* **2007**, *253*, 7041−7045.
(28) Wen, B.; Cao, M.; Lu, M.; Cao, W.; Shi, H.; Liu, J.; Wang, X.; Jin, H.; Fang, X.; Wang, W.; Yuan, J. Reduced Graphene Oxides: Light-Weight and High-Efficiency Electromagnetic Interference Shielding at Elevated Temperatures. *Adv. Mater.* **2014**, *26*, 3484−3489.
(29) Wang, X.; Shu, J.-C.; He, X.-M.; Zhang, M.; Wang, X.-X.; Gao, C.; Yuan, J.; Cao, M.-S. Green Approach to Conductive PEDOT:PSS Decorating Magnetic-Graphene to Recover Conductivity for Highly Efficient Absorption. *ACS Sustainable Chem. Eng.* **2018**, *6*, 14017−14025.
(30) Chen, Y.; Wang, L.; Wang, W.; Cao, M. Enhanced Photoelectrochemical Properties of ZnO/ZnSe/CdSe/Cu_{2-x}Se Core−Shell Nanowire Arrays Fabricated by Ion-Replacement Method. *Appl. Catal. B* **2017**, *209*, 110−117.
(31) Wei, J.; Zang, Z.; Zhang, Y.; Wang, M.; Du, J.; Tang, X. Enhanced Performance of Light-Controlled Conductive Switching in Hybrid Cuprous Oxide/Reduced Graphene Oxide (Cu_2O/RGO) Nanocomposites. *Opt. Lett.* **2017**, *42*, 911−914.
(32) Huang, H.; Zhang, J.; Jiang, L.; Zang, Z. Preparation of Cubic Cu_2O Nanoparticles Wrapped by Reduced Graphene Oxide for the Efficient Removal of Rhodamine B. *J. Alloys Compd.* **2017**, *718*, 112−115.
(33) Liu, X.; Xu, T.; Li, Y.; Zang, Z.; Peng, X.; Wei, H.; Zha, W.; Wang, F. Enhanced X-Ray Photon Response in Solution-Synthesized $CsPbBr_3$ Nanoparticles Wrapped by Reduced Graphene Oxide. *Sol. Energy Mater. Sol. Cells* **2018**, *187*, 249−254.
(34) Ding, Y.; Guo, X.; Kuang, D.; Hu, X.; Zhou, Y.; He, Y.; Zang, Z. Hollow Cu2O Nanospheres Loaded with MoS_2/Reduced Graphene Oxide Nanosheets for Ppb-Level NO2 Detection at Room Temperature. *J. Hazard. Mater.* **2021**, *416*, 126218.
(35) Jiang, R.; Li, B.; Fang, C.; Wang, J. Metal/Semiconductor Hybrid Nanostructures for Plasmon-Enhanced Applications. *Adv. Mater.* **2014**, *26*, 5274−5309.
(36) Wang, Z.; Xing, X.; Yang, Y.; Zhao, R.; Zou, T.; Wang, Z.; Wang, Y. One-Step Hydrothermal Synthesis of Thioglycolic Acid Capped CdS Quantum Dots as Fluorescence Determination of Cobalt Ion. *Sci. Rep.* **2018**, *8*, 8953.
(37) Ding, L.; Fan, C.; Zhong, Y.; Li, T.; Huang, J. A Sensitive Optic Fiber Sensor Based on CdSe QDs Fluorophore for Nitric Oxide Detection. *Sens. Actuators B: Chem.* **2013**, *185*, 70−76.
(38) Abdel Messih, M. F.; Shalan, A. E.; Sanad, M. F.; Ahmed, M. A. Facile Approach to Prepare ZnO@SiO_2 Nanomaterials for Photocatalytic Degradation of Some Organic Pollutant Models. *J. Mater. Sci.: Mater. Electron.* **2019**, *30*, 14291−14299.
(39) Sanad, M. F.; Shalan, A. E.; Bazid, S. M.; Abdelbasir, S. M. Pollutant Degradation of Different Organic Dyes Using the Photocatalytic Activity of ZnO@ZnS Nanocomposite Materials. *J. Environ. Chem. Eng.* **2018**, *6*, 3981−3990.
(40) Nabih, S.; Shalan, A. E.; Serea, E. S. A.; Goda, M. A.; Sanad, M. F. Photocatalytic Performance of TiO_2@SiO_2 Nanocomposites for the Treatment of Different Organic Dyes. *J. Mater. Sci.: Mater. Electron.* **2019**, *30*, 9623−9633.
(41) Jin, J.; Yu, J.; Guo, D.; Cui, C.; Ho, W. A Hierarchical Z-Scheme CdS-WO3Photocatalyst with Enhanced CO2Reduction Activity. *Small* **2015**, *11*, 5262−5271.
(42) Chang, X.; Wang, T.; Gong, J. CO_2 Photo-Reduction: Insights into CO_2 Activation and Reaction on Surfaces of Photocatalysts. *Energy Environ. Sci.* **2016**, *9*, 2177−2196.
(43) Low, J.; Yu, J.; Ho, W. Graphene-Based Photocatalysts for CO_2 Reduction to Solar Fuel. *J. Phys. Chem. Lett.* **2015**, *6*, 4244−4251.
(44) Yadav, P.; Surolia, P. K.; Vaya, D. Synthesis and application of copper ferrite-graphene oxide nanocomposite photocatalyst for the degradation of malachite green. *Mater. Today Proc.* **2021**, *43*, 2949−2953.
(45) Hemmateenejad, B.; Shadabipour, P.; Khosousi, T.; Shamsipur, M. Chemometrics investigation of the light-free degradation of methyl green and malachite green by starch-coated CdSe quantum dots. *J. Ind. Eng. Chem.* **2015**, *27*, 384−390.
(46) Wang, P.; Li, D.; Chen, J.; Zhang, X.; Xian, J.; Yang, X.; et al. A novel and green method to synthesize CdSe quantum dots-modified TiO_2 and its enhanced visible light photocatalytic activity. *Appl. Catal., B* **2014**, *160-161*, 217−226.
(47) Han, G.; Wang, L.; Pei, C.; Shi, R.; Liu, B.; Zhao, H.; et al. Size-dependent optical properties and enhanced visible light photocatalytic activity of wurtzite CdSe hexagonal nanoflakes with dominant {001} facets. *J. Alloys Compd.* **2014**, *610*, 62−68.

https://doi.org/10.1021/acsomega.1c02667
ACS Omega 2021, 6, 23129−23138